The Astrophysical Journal, 681:141–150, 2008 July 1

GEMINI IMAGING OF MID-INFRARED EMISSION FROM THE NUCLEAR REGION OF CENTAURUS A

James T. Radomski,[1] Christopher Packham,[2] N. A. Levenson,[3] Eric Perlman,[4]
Lerothodi L. Leeuw,[5] Henry Matthews,[6] Rachel Mason,[7] James M. De Buizer,[1]
Charles M. Telesco,[2] and Manuel Orduna[2]
Received 2006 November 8; accepted 2008 February 18

ABSTRACT

We present high spatial resolution mid-IR images of the nuclear region of NGC 5128 (Centaurus A). Images were obtained at 8.8 μm, *N* band (10.4 μm), and 18.3 μm using the mid-IR imager/spectrometer T-ReCS on Gemini South. These images show a bright unresolved core surrounded by low-level extended emission. We place an upper limit to the size of the unresolved nucleus of 3.2 pc (0.19″) at 8.8 μm and 3.5 pc (0.21″) at 18.3 μm at the level of the FWHM. The most likely source of nuclear mid-IR emission is from a dusty torus and possibly a dusty narrow-line region with some contribution from synchrotron emission associated with the jet as well as relatively minor starburst activity. Clumpy tori models are presented which predict the mid-IR size of this torus to be no larger than 0.05″ (0.85 pc). Surrounding the nucleus is extensive low-level mid-IR emission. This paper presents to date the highest spatial resolution mid-IR images of this extended near nuclear structure, previously observed by *ISO* and *Spitzer*. Much of the emission is coincident with Paα sources seen by *HST* implying emission from star-forming areas; however, evidence for jet-induced star formation, synchrotron emission from the jet, a nuclear bar/ring, and an extended dusty narrow emission line region is also discussed.

Subject headings: galaxies: active — galaxies: individual (Centaurus A) — galaxies: nuclei — galaxies: Seyfert — infrared: galaxies

1. INTRODUCTION

Centaurus A (NGC 5128, hereafter Cen A) is a nearby elliptical galaxy and the prototypical Fanaroff-Riley type I (FR I) source with spectacular twin radio lobes extending out to $\sim 4^\circ$ ($\sim$250 kpc) from the nucleus (see Israel 1998 for an excellent review). The morphology as well as a bimodal metallicity distribution of the globular cluster population indicate the galaxy has experienced a major merger event in the past (perhaps as recently as 1.6×10^8 yr ago; Quillen et al. 1993). On nuclear scales, evidence for a central supermassive black hole (SMBH) comes from variable X-ray and radio observations. Estimates of the black hole mass by Silge et al. (2005), Marconi et al. (2006), and Häring-Neumayer et al. (2006) suggest it to be $\sim 10^8\ M_\odot$.

Despite intensive studies of Cen A, observations at UV and optical wavelengths have been especially hampered by the dust lane that bisects the galaxy and heavily obscures the nuclear regions. In addition, unified theories of active galactic nuclei (AGNs; Krolik & Begelman 1988; Antonucci 1993; Urry & Padovani 1995) suggest the central SMBH is obscured from our line of sight by a geometrically and optically thick torus of gas and dust that further extinguishes radiation arising from accretion onto the SMBH. High spatial resolution mid-IR observations now available with 8 m class telescopes such as Gemini offer an ideal way to study the obscured central region of Cen A, having extinction 25–75 times lower than observations at optical wavelengths. High spatial resolution mid-IR imaging of other nearby AGNs (e.g., Radomski et al. 2002, 2003; Radomski 2003; Packham et al. 2005; Soifer et al. 2000, 2001, 2003; Perlman et al. 2001; Mason et al. 2007; Alonso-Herrero et al. 2006) highlight the value of such observations in separating and modeling emission from nuclear star formation regions, the torus, and dusty narrow emission line regions.

Previous mid-IR observations of Cen A have produced somewhat contradictory results. Thus, the true nature and extent of the nuclear emission remains controversial. Observations by Whysong & Antonucci (2004) on the Keck I detected an unresolved nucleus at 11.7 and 17.75 μm at resolutions of $\sim$0.3″ and 0.5″, respectively, placing limits of 5.6 and 8.85 pc on the size of the mid-IR emitting region. However, Karovska et al. (2003, hereafter K03) claim to resolve the nucleus of Cen A based on 8.8 μm and *N*-band imaging with the Magellan 6.5 m telescope, calculating a size of $0.17'' \pm 0.02''$ or 3 pc after subtracting a point-spread function (PSF) in quadrature. Further observations by Siebenmorgen et al. (2004) with a resolution of $\sim$0.5″ were unable to directly resolve the nucleus at 10.4 μm, but showed that the growth curve indicated weak extended emission over 2″ with a surface brightness a factor of 10 lower than the peak of the nucleus. Most recently, observations by Hardcastle et al. (2006, hereafter HKW06) find the nuclear FWHM of Cen A to be slightly resolved, calculating a conservative upper limit of 0.27″ or $\leq$4.6 pc at *N* band ($\lambda_0 = 10.4$ μm). If the nucleus of Cen A is resolved, this could be the first galaxy in which the emission from dust associated with the torus has been resolved with single-telescope mid-IR observations. In order to address the controversy of the central nuclear resolution of Cen A, we have methodically observed Cen A and corresponding calibration sources at high resolution in the mid-IR to (1) test the hypothesis that the nucleus is resolved and (2) characterize the

[1] Gemini South Observatory, Casilla 603, La Serena, Chile.
[2] Astronomy Department, University of Florida, 211 Bryant Space Science Center, P.O. Box 112055, Gainesville, FL 32611-2055.
[3] Department of Physics and Astronomy, University of Kentucky, Lexington, KY 40506.
[4] Joint Center for Astrophysics, Department of Physics, University of Maryland, Baltimore County, 1000 Hilltop Circle, Baltimore, MD 21250.
[5] Department of Physics and Electronics, Rhodes University, P.O. Box 94, Grahamstown 6140, South Africa.
[6] Herzberg Institute of Astrophysics, National Research Council, P.O. Box 248, Penticton, BC V2A 6J9, Canada.
[7] Gemini North Observatory, 670 North A'ohoku Place, Hilo, HI 96720.

mid-IR emission mechanisms. In addition, we draw upon publicly accessible archived observations in the mid-IR in addition to our own data to further explore low-level extended emission surrounding the nucleus of Cen A. Our observations are discussed in § 2, while results and analysis are presented in §§ 3 and 4, respectively. Throughout this paper we assume a distance to Cen A of $D = 3.5$ Mpc ($1'' = 17$ pc).

2. OBSERVATIONS AND DATA REDUCTION

Observations of Cen A were made over two epochs. Epoch A occurred on 2004 January 28 and 29 (UT) and was initiated by the authors of this paper. Epoch B was observed on 2004 March 6, 11, and 12 and was retrieved from the Gemini Science Archive (GSA) based on data first published by HKW06. Both sets of data were obtained using the facility mid-IR camera/spectrograph T-ReCS (Thermal-Region Camera Spectrograph; Telesco et al. 1998) on the Gemini South telescope. T-ReCS uses a Raytheon 320×240 pixel Si:As IBC array, providing a plate scale of $0.089''$ pixel^{-1}, corresponding to a field of view of $28.5'' \times 21.4''$. The detector was read out in correlated quadruple sampling (CQS) mode (Sako et al. 2003). The standard chop-nod technique was used to remove time-variable sky background, telescope thermal emission, and the so-called 1/f detector noise. The chop throw was $15''$, and the telescope was nodded every 30 s. All data were reduced using IDL.

2.1. *Epoch A: 2004 January 28 and 29*

We carefully observed Cen A over a period of two nights. Images were obtained in the Si-2 ($\lambda_0 = 8.74$ μm, $\Delta\lambda = 0.78$ μm) and Qa ($\lambda_0 = 18.3$ μm, $\Delta\lambda = 1.5$ μm) filters to optimize resolution and sensitivity in both the 10 and 20 μm atmospheric windows. The chop and nod direction was fixed at 0° (north-south). The first night we observed at 8.8 μm for about 3.5 hr real-time (real time $\sim 3.5 \times$ on-source time due to chop-nod procedure, not including time for telescope slewing and calibration) using an iterative procedure which repeatedly interleaved observations of a PSF star (65 s on-source) with those of Cen A (455 s on-source). This resulted in a total of five PSF observations (5.4 minutes on-source total) and five galaxy observations (34 minutes on-source total). We used the same procedure on the second night at 18.3 μm; however, the initial PSF star had too low a signal-to-noise ratio (S/N), so a new PSF was chosen resulting in only three high-S/N PSF measurements (3.3 minutes on-source total). A total of four galaxy observations (26.4 minutes on-source total) at 18.3 μm were obtained. Estimates of the FWHM of the galaxy and PSF were done by fitting a Moffat function (Moffat 1969).

The stars PPM 318494 and PPM 291667, located 1.5° and 4.2° from Cen A, were used for PSF comparison to look for extended emission in the galaxy. Each of the PSF observations was made immediately prior to or after the Cen A observations and using an identical observational setup to accurately sample the delivered image quality of those observations. PSF images were not rotated to correct for changes in the pupil due to the small rotation angle of the pupil between observations of the galaxy and PSF (typically $<6°$). This was done to avoid the slight smoothing of the FWHM that occurs when an image is digitally rotated to correct for pupil rotation. Line cuts taken at similar pupil angles on the galaxy justify this. These showed the profiles to be radially symmetric; hence, an azimuthally averaged FWHM was adequate for investigating any resolved emission in the nucleus of Cen A.

Observations of HD 110458 were used for flux calibration through both Si-2 and Qa filters at an air mass similar to that for the Cen A observations. Absolute calibration was achieved using the TIMMI2 photometric standard list, where the flux densities of HD 110458 at 8.8 and 18.3 μm are 6.95 and 1.72 Jy, respectively. Observations of HD 110458 and Cen A at 8.8 μm show variations of $\lesssim 5\%$. At 18.3 μm only one observation of the flux calibrator was taken. However, observations of the relative flux of Cen A at 18.3 μm showed variations of $\sim 25\%$.

The differences in the intrinsic spectra of the stellar sources and Cen A as observed through the Si-2 and Qa filters requires a color correction. This color correction affects not only the observed fluxes but also the FWHM. A stellar spectrum peaking at shorter wavelengths ($T \sim 4000$ K) will dominate the shorter wavelength portion of the filter. A cooler source such as Cen A ($T \sim 200$ K) will peak at longer wavelengths and dominate the longer wavelength portion of the filter. The resulting effect will not only alter the flux calibration but also cause the FWHM of "hot" stellar sources to be smaller than the relatively "cool" Cen A when observed through the same filter. This effect is significant in large-bandpass mid-IR filters such as *N* band ($\lambda_0 = 10.4$ μm, $\Delta\lambda = 5.3$ μm). The difference between a $T \sim 4000$ and ~ 200 K source in the *N* band will result in a color correction of the observed flux density up to 21%, and the observed FWHM of the stellar source will appear 12% smaller. Due to the relatively small bandwidth of the Si-2 and Qa filters ($\Delta\lambda = 0.78$ and 1.5 μm) this effect is much smaller. The color correction between a $T \sim 4000$ and 200 K source is $<4\%$ and the difference in the FWHM is $<0.05\%$, both within the errors of our observations.

2.2. *Epoch B: 2004 March 6, 11, and 12*

Epoch B data were first published by HKW06 and were retrieved from the GSA after their proprietary period to compare with our observations. Images were obtained in the *N* band ($\lambda_0 = 10.4$ μm, $\Delta\lambda = 5.3$ μm) over the nights of 2004 March 6, 11, and 12. The chop angle was 121°, and the instrument position angle (P.A.) was set at 172°. The nucleus was positioned in the corner of the array in order to concentrate on possible extended mid-IR emission along the synchrotron jet emanating from the AGN. On March 6, HD 110458 was observed for a PSF and flux calibrator (43 s on-source) followed by six successive observations of Cen A (each 825 s on-source) for a total on-source time of 82.5 minutes on the galaxy. On the following night of observations, March 11, Cen A was observed twice (each observation 825 s on-source) followed by a PSF and calibrator star HD 108903 (36 s on-source). The same observation sequence was repeated on March 12.

3. RESULTS

In both epochs A and B we detect low-level extended mid-IR emission near the nucleus of Cen A at 8.8 μm, *N* band, and 18.3 μm. Using multiple observations of the AGN and nearby stellar targets in epoch A we determine the central nucleus of Cen A to be unresolved at both 8.8 and 18.3 μm and place firm limits on the size based on the FWHM. We make a distinction between the unresolved nucleus and the surrounding emission and discuss both separately in §§ 3.1 and 3.2, followed by analysis of the source of such emission in § 4. Table 1 lists our photometry in comparison to others in the literature.

3.1. *The Central Nucleus*

Figure 1 shows the FWHM of the nucleus of Cen A and corresponding PSFs over time. Observations of the galaxy were split up into nod-sets to match the same integration times of the PSF for careful comparison (65 s on-source at 8.8 μm and 109 s on-source at 18.3 μm). The overall decrease in FWHM in the

TABLE 1
CEN A FLUX DENSITY MEASUREMENTS

Reference	Wavelength (μm)	Telescope	Resolution (arcsec)	Flux Density (Jy)	Time On-Source (s)
This paper	8.8	Gemini South (8 m)	0.30	0.71 ± 0.04[a]	2000
	18.3	Gemini South (8 m)	0.53	2.63 ± 0.65[a]	1550
Karovska et al. (2003)	8.8	Magellan (6 m)	0.45	0.9 ± 0.1	1400
	10 (*N* band)	Magellan (6 m)	0.45	1.4 ± 0.5	900
Siebenmorgen et al. (2004)	10.4	ESO (3.6 m)	0.5	0.65 ± 0.065	645
Krabbe et al. (2001)	10 (*N* band)	ESO MPI (2.2 m)	1	0.75 ± 0.055	600
Hardcastle et al. (2006)	10 (*N* band)	Gemini South (8 m)	0.4	1.1 ± 0.11	8250
Whysong & Antonucci (2004)	11.7	Keck I (10 m)	~0.3	1.6 ± 0.2	...
	~11.7 (SiC)	Keck I (10 m)	~0.3	1.8 ± 0.2	...
	17.75	Keck I (10 m)	~0.5	2.3 ± 0.2	...

[a] Errors in flux density are dominated by uncertainty in calibration ($\leq$5% at 8.8 μm and $\leq$25% at 18.3 μm) but also include a small statistical error based on the aperture size.

8.8 μm plot corresponds to the lower air mass through the observations as well as an improvement in seeing throughout the night. A similar plot is also shown for 18.3 μm in Figure 1. Although there is some variation in the FWHM, the bright nucleus of Cen A is unresolved. Figure 2 shows azimuthally averaged radial profiles of the total co-added Cen A data at 8.8 and 18.3 μm

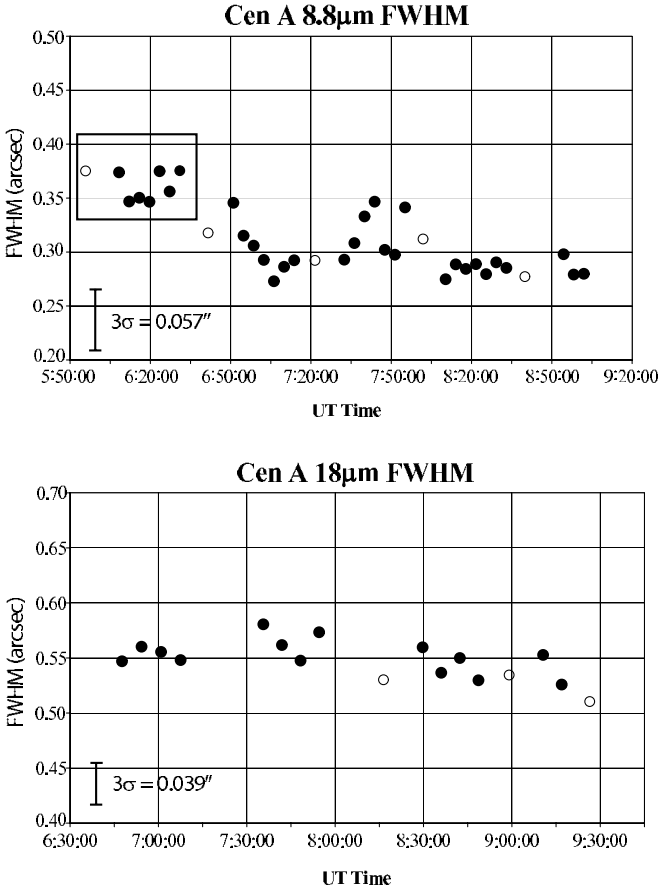

FIG. 1.—FWHM of Cen A (*filled circles*) in comparison to that of the PSF (*open circles*) vs. the time observed each night for 8.8 μm (*top*) and 18.3 μm (*bottom*). Each circle corresponds to equal time intervals for galaxy and PSF (65 s on-source at 8.8 μm and 109 s on-source at 18.3 μm). The box in the 8.8 μm figure (*top*) indicates data taken at high air mass and relatively poor seeing that was not used in the overall analysis. In some cases the galaxy observations contained slightly more time left over after being divided into intervals equal to that of the PSF (<22 s on-source). In these cases the data were not plotted as they were of short enough duration and did not add any new information to the analysis.

in comparison to the co-add of all the PSF observations at each wavelength. Given the 3 σ variation of the PSF it is clear the bright nucleus of Cen A is unresolved at both wavelengths. Neither the extension claimed by K03 nor that by HKW06 is detected. In the case of K03 it was noted that several hours passed between galaxy and PSF observations, while HKW06 compared individual galaxy exposures of 825 s on-source with a single short 43 s on-source observation of the PSF. As can be seen in Figure 1, the PSF and galaxy vary significantly over time with changes in seeing and air mass, highlighting the potential dangers in comparing a single, short PSF measurement to a set of longer galaxy observations.

We agree with the observations of Whysong & Antonucci (2004) that the nucleus of Cen A is unresolved, although with multiple PSF observations we are able to place a tighter statistical constraint of the size of the bright mid-IR nucleus. Following the analysis of Soifer et al. (2000) and Packham et al. (2005), we suggest that any nuclear extensions would be readily detected at 3 times the standard deviation of the PSF standard. For our 8.8 μm data the median size of the PSF $\theta_{\rm PSF} = 0.3''$, 3 $\sigma = 0.057''$ ($\theta_{\rm sd}$), which excludes the first PSF observation taken under poor seeing and high air mass that is not representative of the group. For our 18.3 μm data median size of the PSF $\theta_{\rm PSF} = 0.53''$, 3 $\sigma = 0.039''$ ($\theta_{\rm sd}$), based on all three PSF observations. The maximum angular extension ($\theta_{\rm max}$) is defined as

$$\theta^2_{\rm max} = \theta^2_{\rm tot} - \theta^2_{\rm PSF}, \quad (1)$$

where $\theta^2_{\rm tot}$ is $(\theta_{\rm PSF} + \theta_{\rm sd})^2$. Thus, any bright nuclear extended emission must occur on scales $<0.19''$ ($\lesssim$3.2 pc) at 8.8 μm and $<0.21''$ ($\lesssim$3.5 pc) at 18.3 μm at the level of the FWHM.

3.2. *The Extended Emission*

Although the mid-IR nucleus of Cen A is unresolved when compared to the FWHM of corresponding PSFs there is clear evidence of surrounding low-level extended emission detected in both epochs A and B. This mid-IR emission is faint and only becomes apparent after a 10 pixel (0.89″) Gaussian smooth is applied. Figure 3 clearly shows this emission at 8.8 and 18.3 μm from epoch A overlaid on Paα emission observed by Marconi et al. (2000). Similar structure to that at 8.8 μm is seen in *N*-band data from epoch B (Fig. 4). This emission has no effect on the FWHM of the central nucleus and could not have been the cause of previous detections of a "resolved" nucleus by K03 or HKW06. It also is too faint, >250 times fainter than the peak at

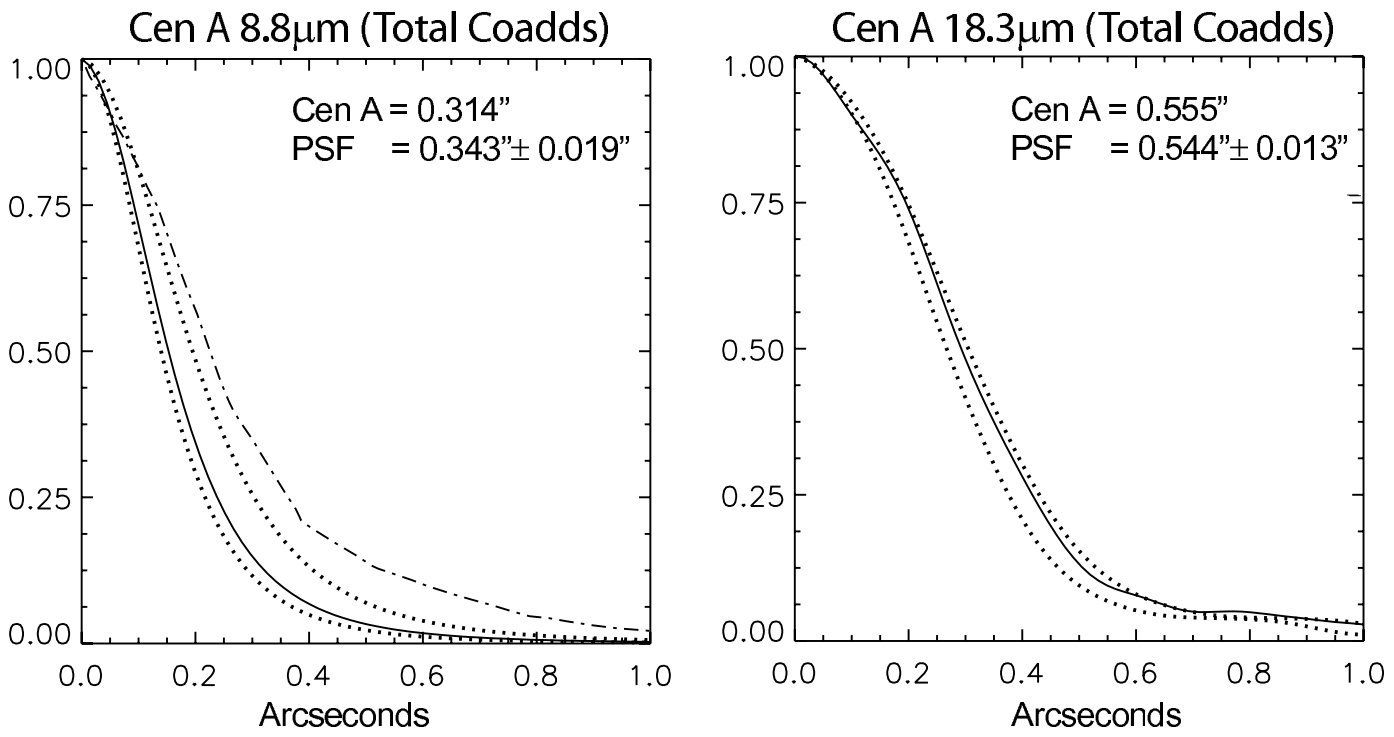

FIG. 2.—Azimuthally averaged radial profiles of Cen A in comparison to the PSF. Solid lines represent the galaxy, while dotted lines represent the 3 σ upper and lower limit in the PSF FWHM size based on the total standard deviation of the PSFs at each wavelength. These images represent a comparison of the fully stacked galaxy data (33.3 minutes on-source at 8.8 μm, *left*; 25.8 minutes on-source for 18.3 μm, *right*) compared to a stack of all PSFs that were taken between galaxy observations. The dash-dotted line represents the measurement of Cen A at 8.8 μm from Fig. 2 of K03. Our 3 σ upper on the PSF is very close to their single PSF measurement. Thus, their 0.17″ size measurement is likely due to seeing.

both 8.8 μm and *N* band of the 10 pixel smoothed image, to be associated with the 2″ extended emission claimed by Siebenmorgen et al. (2004), which was only at a level of 1/10 the peak at 10.4 μm (Fig. 5).

Low-level extended mid-IR emission is known to exist near the nucleus of Cen A. Observations using the *Infrared Space Observatory* (*ISO*) by Mirabel et al. (1999) and most recently *Spitzer* observations by Quillen et al. (2006a, 2006b) show the nucleus is surrounded by a dusty warped disk. Observations in this paper, however, represent to date the highest resolution mid-IR images that clearly detect this emission surrounding the nucleus. But analysis of this emission is limited due to the chop throw of 15″, which results in some chopping onto emission, compromising detailed examination of the flux and morphological parameters. Although it is a minor effect with respect to the bright nucleus, the faint extended emission does show some evidence of negative chop regions. However, the similar mid-IR structure of this emission at 8.8 μm and *N* band despite chopping onto different regions would seem to show that much of the structure observed is real. In addition, the correspondence of the mid-IR with

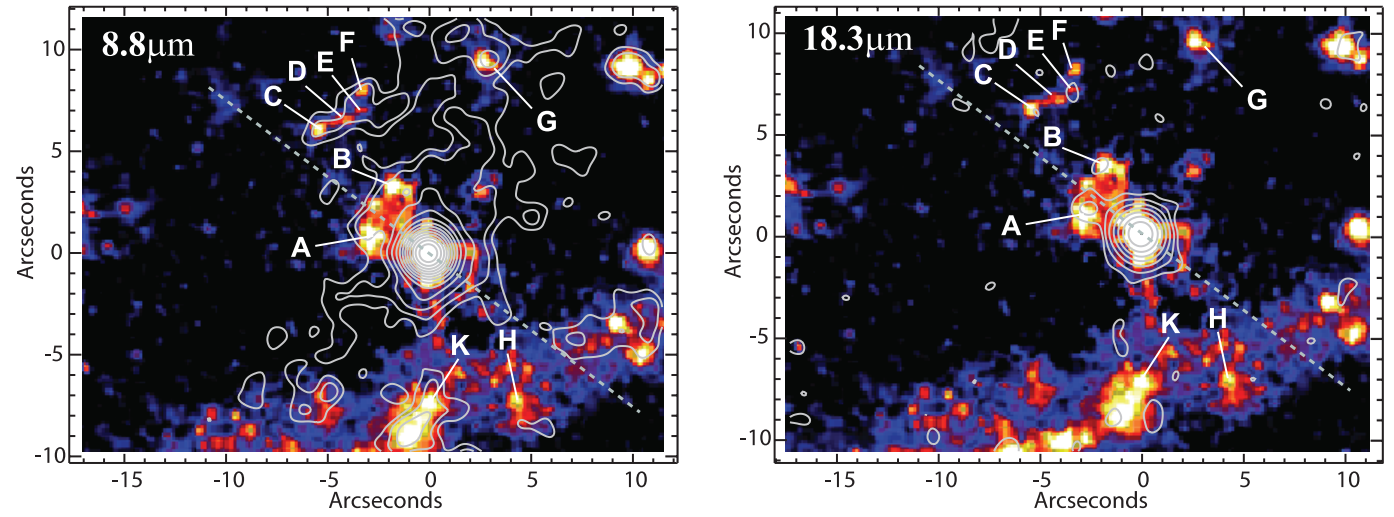

FIG. 3.—Paα emission from *HST* (Marconi et al. 2000), overlaid with contours representing our heavily smoothed (10 pixel Gaussian =0.89″) mid-IR data at 8.8 μm (*left*) and 18.3 μm (*right*). Contours are logarithmic with a factor of 1.66 (8.8 μm) and 2.11 (18.3 μm) between them. The lowest contours represent 2 σ above the smoothed background (0.006 mJy pixel^{-1} at 8.8 μm and 0.066 mJy pixel^{-1} at 18.3 μm). Letters represent the bright Paα emission regions detected by Schreier et al. (1998). The dotted line represents the approximate angle of the radio jet axis (P.A. = 53°).

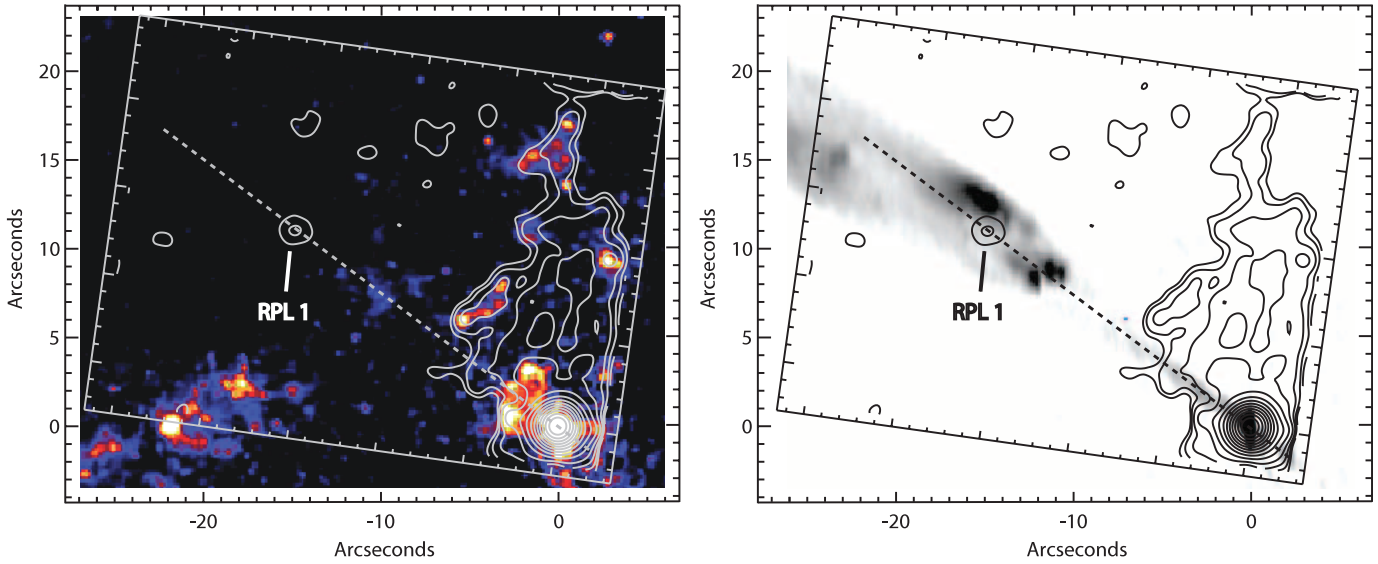

FIG. 4.—*Left*, Paα map from Marconi et al. (2000) as in Fig. 3; *right*, gray-scale radio map of Hardcastle et al. (2003). Contours represent a stack of *N*-band data from all three nights (2004 March 6, 11, and 12) retrieved from the GSA archive and are logarithmic with a factor of 1.79 between them. The lowest contours represent 2 σ above the smoothed background (0.0034 mJy pixel^{-1}). The mid-IR source RPL 1 is detected coincident with the approximate radio jet P.A. = 53° (*dotted line*).

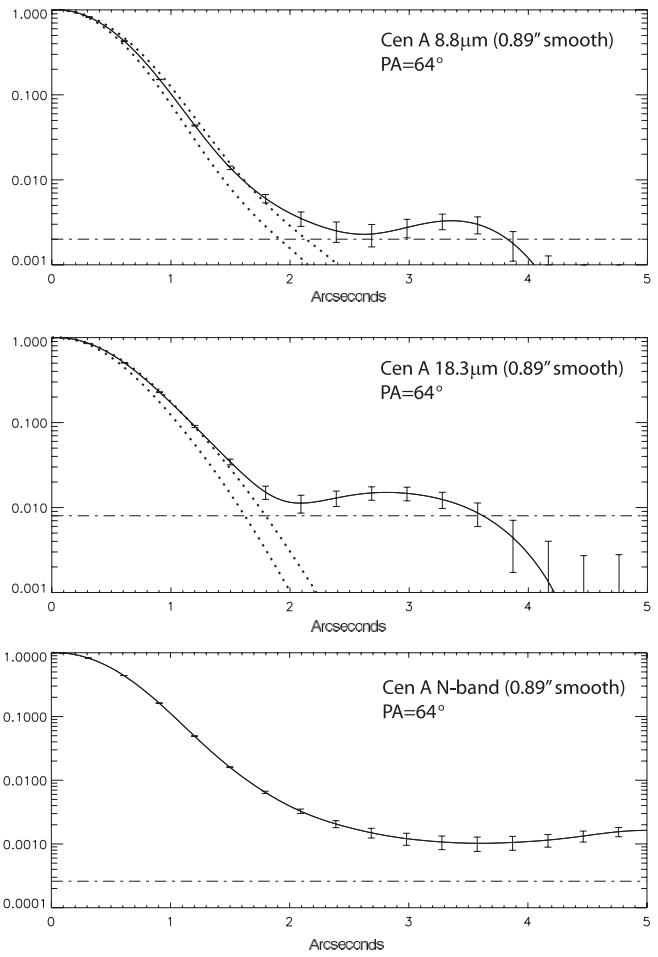

FIG. 5.—Line cuts of Cen A at a P.A. = 64° after a 10 pixel (0.89″) Gaussian smooth. Solid and dotted lines represent the same as Fig. 2. The dash-dotted line represents 3 σ above the background, and error bars represent ±1 σ of the background. The position angle is along the extended emission clump detected at 18.3 μm near Paα source A from Schreier et al. (1998) and close to the jet axis. Low-level emission near this clump is clearly detected at 8.8 μm, 18.3 μm, and *N* band greater than 3 σ above the background.

emission regions of Paα detected by Schreier et al. (1998) and Marconi et al. (2000) reinforces that in fact what we see are primarily real structures (Figs. 3 and 4).

4. ANALYSIS: SOURCES OF EMISSION

In this section we discuss the possible origins of the mid-IR emission of both the bright unresolved central nucleus and the low-level extended emission. Due to the contamination from chopping onto nearby emission, the analysis of the low-level extended emission is presented in a broad overview. Additional imaging data resulting in a more detailed analysis of this emission will be put forth by L. L. Leeuw et al. (in preparation).

4.1. *The Nucleus*

4.1.1. *Nucleus: Stellar Activity*

Starburst activity in the nucleus of Cen A has been modeled by Alexander et al. (1999), who fit the nuclear (<4″) IR flux ≤60 μm with approximately equal parts dusty torus and starburst emission. However, their nuclear starburst component depends strongly on fitting the 11.3 μm polycyclic aromatic hydrocarbon (PAH) feature from Mirabel et al. (1999) that is not seen in the higher spatial resolution (∼3″) Siebenmorgen et al. (2004) data. In addition, estimates of the high intrinsic polarization from near-IR observations by Packham et al. (1996) and Capetti et al. (2000) on the order of 11%–17% are consistent with optically thin scattering from a compact torus surrounding the central engine rather than a starburst.

Combining our data with bolometric luminosity measurements, we can evaluate the likely contribution of a starburst using a "luminosity density" analysis similar to that by Soifer et al. (2000, 2001, 2003) and Evans et al. (2003). They have calculated the surface brightnesses from infrared luminous AGNs and starburst galaxies. This was done by measuring the size or upper limit of the mid-IR size of a compact region and assuming that this mid-IR region is representative of the infrared emitting region as a whole. Using the total IR luminosity as an approximation of the bolometric luminosity in these galaxies and assuming it originates from this region resulted in an estimate of the luminosity density. In general, they found that Galactic H II regions have

surface brightnesses ranging from 2×10^{11} to 2×10^{12} $L_{\odot}$ kpc^{-2}, starburst galaxies range from 2×10^{11} to 10^{13} $L_{\odot}$ kpc^{-2}, while ULIRGs (ultraluminous infrared galaxies) typically range from 2×10^{12} to 6×10^{13} $L_{\odot}$ kpc^{-2}. On small scales ($\leq$10 pc) Meurer et al. (1997) found that star clusters may have a global (UV, IR, and radio) surface brightness as high as 5×10^{13} $L_{\odot}$ kpc^{-2}. Soifer et al. (2003) found in three Seyfert galaxies surface brightnesses on the order of a few $\times 10^{14}$ $L_{\odot}$ kpc^{-2}, which they argued must be primarily AGN emission, being well above the luminosity density of bright star clusters and starbursts.

Based on our observations we measure a mid-IR luminosity of the nucleus of Cen A of 1.8×10^{8} $L_{\odot}$. This value is similar to the 1.5×10^{8} $L_{\odot}$ value of Whysong & Antonucci (2004) based on their 11.7 μm measurement and represents a lower limit to the total luminosity. Assuming a normal quasar spectral energy distribution (SED) Whysong & Antonucci (2004) estimate the bolometric luminosity of the AGN to be $\sim 2.5 \times 10^{9}$ $L_{\odot}$. This is similar to the value calculated by Israel (1998) and within a factor of $\sim$2 of that quoted by Marconi et al. (2001a). Given the lower estimated bolometric luminosity and our maximum size limit of 3.5 pc from our 18.3 μm observations we calculate a luminosity density for Cen A of 2.8×10^{14} $L_{\odot}$ kpc^{-2}. These values are similar to those found by Soifer et al. (2003) for Seyfert galaxies in which starburst activity was considered negligible in regions with a luminosity density $>10^{14}$ $L_{\odot}$ kpc^{-2}. Even a bright star cluster as suggested by Meurer et al. (1997; 5×10^{13} $L_{\odot}$ kpc^{-2}) could only contribute $<$18% to the overall luminosity density. Thus, this general analysis in addition to the lack of PAH emission detected by Siebenmorgen et al. (2004) and the strong polarization observations obtained by Packham et al. (1996) and Capetti et al. (2000) indicate that any starburst activity in the nucleus of Cen A is negligible compared to the emission from the AGN.

4.1.2. *Nucleus: Narrow-Line Region (NLR) Dust*

In order to explore the possibility of central heating of a dusty NLR we calculate color temperatures from the ratio of our 8.8 and 18.3 μm fluxes (see Radomski et al. 2003). Based on this ratio we calculate a temperature of the nucleus of $\sim$210 K. A similar temperature is obtained if we use the ratio of fluxes at 11.7 and 17.75 μm from Whysong & Antonucci (2004). This value is slightly higher than the $\sim$160 K calculated by K03 based on their single 8.8 μm flux. However, we can achieve approximately the same temperature using their formula for our 8.8 μm measurement, so the difference is entirely due to the calculation method. Taking into account extinction from the dust lane across Cen A as proposed by K03 of $\tau \sim 1$ at 10 μm raises the color temperature by only 20 K to 230 K.

We derive an approximation of the dust grain properties using the methodology applied to NGC 4151 (Radomski et al. 2003) and Circinus (Packham et al. 2005). Assuming a simple uniform dust distribution, a first-order determination of the size of the region that could be heated by a central source can be made. Given that dust grains primarily absorb UV-optical radiation and reemit in the infrared, the equilibrium temperature of dust in a strong UV field is given by (Sellgren et al. 1983)

$$T \sim \left(\frac{L_{\rm UV}}{16 \pi R^2 \sigma} \frac{Q_{\rm UV}}{Q_{\rm IR}} \right)^{1/4}. \quad (2)$$

In the above equation, T is the dust temperature, $L_{\rm UV}$ is the approximate UV-optical luminosity of the central source, R is the radius from the source in parsecs, σ is the Stefan-Boltzmann constant, and $Q_{\rm UV}/Q_{\rm IR}$ is the ratio of the Planck-averaged UV absorption coefficient to the infrared emission coefficient. Values of $Q_{\rm UV}/Q_{\rm IR}$ are dependent on the dust grain size and composition and are given by Draine & Lee (1984), Laor & Draine (1993), and Weingartner & Draine (2001) for graphite and "smoothed astronomical" (SA) silicate.

Using the bolometric luminosity of 2.5×10^{9} $L_{\odot}$ as an estimate and a dust temperature of 200 K, Cen A could heat NLR dust similar to that in Circinus and NGC 4151 (0.003–0.01 μm silicate; 0.015–0.04 μm graphite) up to a radial distance of 9–14 pc ($\sim$0.5″–0.8″) from the central engine. This is much larger than the maximum size of the unresolved mid-IR nucleus (0.21″; 3.5 pc diameter) and shows that the central AGN is capable of heating all the dust in the core. With these observations it is difficult to determine how much of this unresolved emission may be distributed between a compact NLR and torus. However, if we assume a scenario similar to that in NGC 4151, then the NLR may only contribute $\sim$10%–20% of the mid-IR emission (Radomski et al. 2003; Groves et al. 2006).

4.1.3. *Nucleus: Dusty Torus*

The maximum size we obtain for the mid-IR emission from dust associated with a compact geometrically and optically thick torus at the level of the FWHM is $<$0.19″ ($\lesssim$3.2 pc) at 8.8 μm and $<$0.21″ ($\lesssim$3.5 pc) at 18.3 μm. This is consistent with observations at K band (2.2 μm) of FWHM $<$ 0.2″ ($<$3.4 pc; Schreier et al. 1998) as well as the polarization observations of Capetti et al. (2000), which suggest scattering off a 2 pc disk. It is also close to the 4.07 pc $\times$ 3.05 pc (scaled to 3.5 Mpc) torus modeled by Alexander et al. (1999), although as discussed above their starburst fit may not be accurate if there is no nuclear PAH emission.

Applying the recent models of Nenkova et al. (2002), we in fact predict that the mid-IR emission of the Cen A torus is unresolvable in the present observations. These models are far more robust than our earlier calculations of dust in the relatively optically thin NLR, taking into account radiative transfer and cloud shadowing necessary in the optically thick environment of a torus. In these models the inner radius of the torus scales with the square root of the AGN luminosity and inversely with temperature to the 5/2 power. At the dust sublimation temperature (1200 K), the inner radius of the Cen A torus may be only 0.07 pc. While the outer edge of the torus may be large ($\sim$5 pc), in these inhomogeneous torus models the cloud distribution declines rapidly ($\propto r^{-q}$, where $q = 1$, 2, or 3). Thus, most of the clouds are strongly concentrated within the inner parsec (Fig. 6). And although the hottest dust has $T = 1200$ K, the contributions of the many cooler indirectly heated clouds are significant, and the net spectrum of the clumpy torus appears much cooler. For the models presented above, F_{ν} peaks around 25 μm, with the color temperature of the 8.8 μm/18.3 μm flux density ratio indicating $T \approx 200$ K.

The model mid-IR emission does not always trace the cloud distribution. Because of the large optical depths through the densest regions of the torus, the heating and subsequent emission can be suppressed in the torus midplane. These effects are strongest at shorter wavelengths and for less compact cloud distributions, where the strongest observable emission extends along the torus axis. In such instances, some hot, luminous material (on the projected front or rear of the torus) is not completely obscured. We modeled a range of torus parameters, which include the radial distribution, q, the optical depth per cloud measured in the V band,

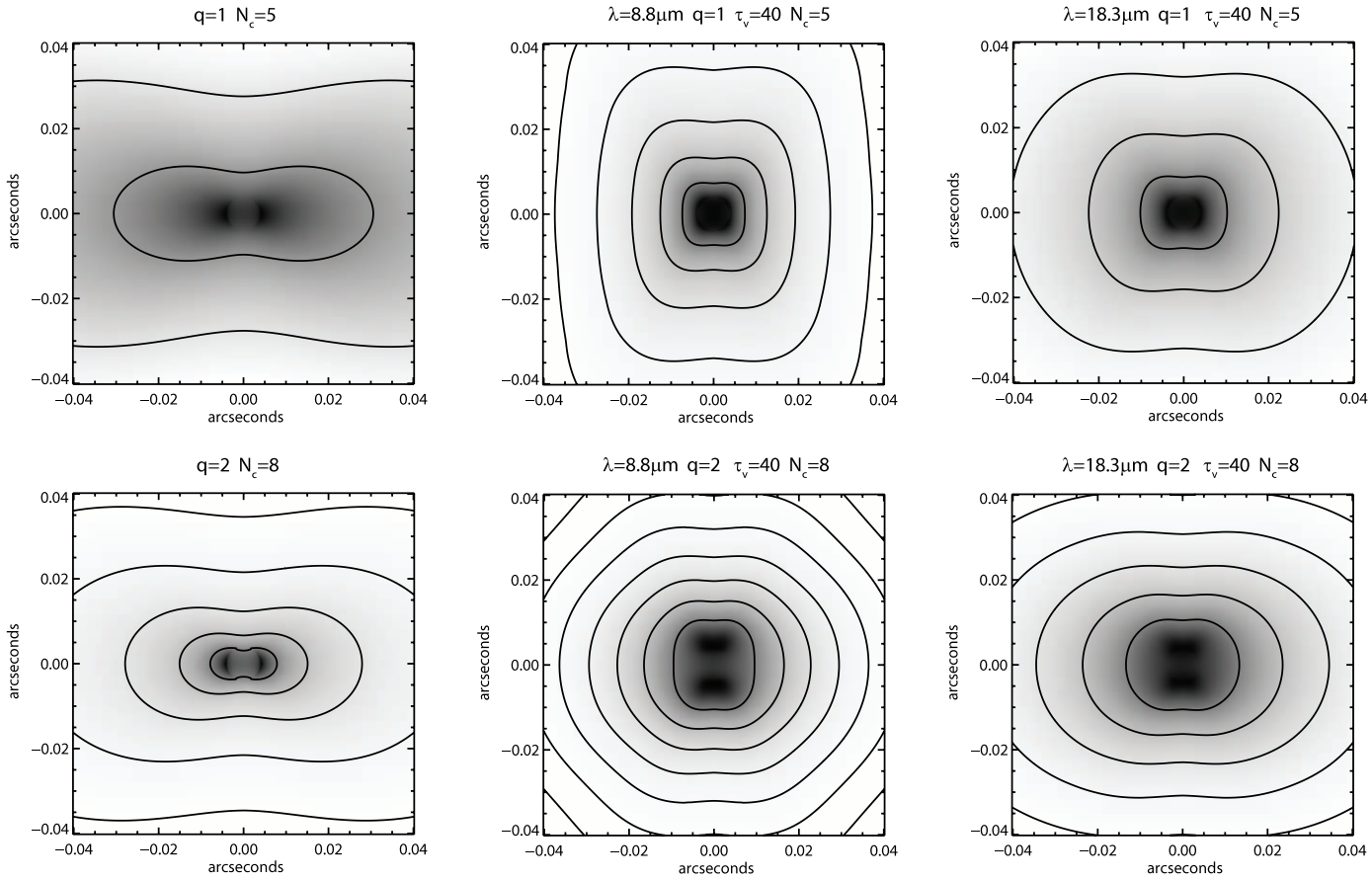

FIG. 6.—Number of clouds integrated along the line of sight, for radial distribution $q = 1$ (*top left*) and $q = 2$ (*bottom left*). For the total number of clouds along an equatorial ray to the central engine, $N_C = 5$ (*top left*) and $N_C = 8$ (*bottom left*), the maximum number of clouds along the line of sight is 12 and 25, respectively, for maximum integrated optical depth of 480 and 1000 in the V band. Beside these cloud distributions are simulated images of emission at 8.8 μm (*middle*) and 18.3 μm (*right*). In these models, the optical depth per cloud $\tau_V = 40$ and the outer radius of the cloud distribution is located at 30 times the dust sublimation radius. The 18.3 μm images of both models are similar to each other and to the cloud distribution because both the heating and subsequent emission are insensitive to optical depth effects. In contrast, the 8.8 μm emission does not trace the cloud distribution because of the large optical depth of the torus and the strong temperature dependence, especially when the distribution is not compact ($q = 1$). Here the emission extends along the polar axis, which is the location of clouds that directly view the AGN and that are not blocked along the line of sight. In all cases, the emission is confined to scales much smaller than the spatial resolution of our observations. The images are scaled linearly, and the contours are logarithmically spaced, beginning at 50% of the peak value and declining by factors of 2.

τ_V, and the total number of clouds through the equatorial plane, N_C. We show the results for a model that fits the observed 10 μm nuclear spectrum of NGC 1068 well (Mason et al. 2006), with $q = 2$ and $N_C = 8$, and a comparison model in which $q = 1$ and $N_C = 5$. In both models, $\tau_V = 40$, the outer radius is 30 times the dust sublimation radius, and the cloud distribution is Gaussian in elevation above the torus midplane, without a sharp cutoff. These two sets of parameters yield cloud distributions and images that are characteristic of the full parameter space we explored.

The torus is viewed edge-on in the simulated images at 8.8 and 18.3 μm (Fig. 6). The 18.3 μm emission generally traces the cloud distribution because optical depth effects are not significant, both for heating the clouds and for their subsequent emission. Directly heated clouds that are not blocked along the line of sight dominate the emission at 8.8 μm. The resulting images are extended perpendicular to the cloud distribution, and in the less compact ($q = 1$) distribution, this extension persists on larger scales. The exact emission profile does depend on the model parameters, but in all cases the strong extended emission (which the FWHM of the simulated images themselves indicates) is confined to scales of 0.02″. In the simulations, the flux declines to 10% of the peak strength on scales of 0.08″ or less. In general, the emission is more compact in the steeper cloud distributions, and it is always much smaller than the 0.2″ upper limit we measure in the data. This approaches the scales of *HST* Space Telescope Imaging Spectrograph (STIS) observations of Marconi et al. (2006), which indicate the central dark object in Cen A is no more than 0.036″–0.04″ (0.6–0.7 pc) in radius. Thus, careful interferometry will be required to resolve this structure.

4.1.4. *Nucleus: Synchrotron Emission*

As in the case of M87 (Perlman et al. 2001), the powerful radio jet of Cen A could provide a significant fraction of the mid-IR emission through synchrotron radiation. Chiaberge et al. (2001) claim the entire nuclear SED of Cen A can be fit with a synchrotron self-Compton (SSC) model. In addition, recent mid-IR interferometry models by Meisenheimer et al. (2007) suggest a tiny predominantly SSC core (<0.2 pc). They model an SSC core contributing between 80% and 60% of the emission between 8 and 13 μm, respectively. However, there are several problems with this scenario.

First, the lack of polarization at ~1000 μm (Packham et al. 1996) is difficult to reconcile with a predominantly synchrotron core. Second, Meisenheimer et al. (2007) reference the variability seen at L band (~3.5 μm) by Lepine et al. (1984) detailing an increase in flux by a factor of 5 between 1971 and 1981 as

evidence of the variable synchrotron nature of the IR core. If the mid-IR core is dominated by synchrotron emission then similar variability should be seen at $\sim$10 μm. However, mid-IR (10 μm) measurements taken coincident with the *L*-band observations (Becklin et al. 1971; Kleinmann & Wright 1974; Grasdalen & Joyce 1976) seem inconsistent with variability trends seen at X-ray and radio wavelengths (Beall et al. 1978; Abraham et al. 1982). Indeed Telesco (1978), comparing mid-IR (10 μm) observations from 1971 to 1978, concluded that there was no evidence of mid-IR variability during this period. Comparing mid-IR observations taken from 1984 to 2004 also shows no significant variation at $\sim$10 μm after accounting for filter and calibration differences (Alexander et al. 1999; Mirabel et al. 1999; Krabbe et al. 2001; Siebenmorgen et al. 2004; K03; Weedman et al. 2005; HKW06; this paper). And finally, the fluxes measured by Meisenheimer et al. (2007) for the SSC core at 11.4 μm are a factor of $\sim$4 smaller that the unresolved core measured by Whysong & Antonucci (2004) at 11.7 μm. Given that the high spatial resolution Siebenmorgen et al. (2004) spectra show no PAH emission it is unlikely that this could affect the flux. Thus, at least at the longer portion of the 10 μm window it appears that there is ample excess emission possibly from a torus that could dominate the mid-IR on scales $<0.3''$.

Another method to estimate the synchrotron emission in the nucleus of Cen A is to use a simple power-law model such as that used for M87 (Perlman et al. 2001). A strong linear correlation between the optical and radio core values of FR I galaxies found by Chiaberge et al. (1999) hinted at a common synchrotron origin for this emission. Capetti et al. (2000) used this correlation and the radio core flux of Cen A of 9.1 Jy at 15 GHz (Clarke et al. 1992) to predict the synchrotron emission at 2 μm of 10 mJy. This trend also follows closely with the synchrotron models of HKW06 which fit the nonnuclear "inner," "middle," and "outer" lobes of the radio jet in Cen A. Assuming this trend and a radio core flux of 9.1 Jy we predict a nonthermal mid-IR flux density between 8 and 18 μm of 30–50 mJy, more than an order of magnitude less than what is measured. This may indicate that synchrotron emission in the nucleus of Cen A is negligible in the mid-IR in comparison to emission from dust.

4.2. *The Extended Emission*

4.2.1. *Extended: Stellar Activity*

The nucleus of Cen A is most likely dominated by the AGN, but much of the surrounding extended emission is likely due to stars. The close correspondence between much of this emission $\gtrsim 5''$ from the nucleus at 8.8 μm and *N* band and the Paα data from Marconi et al. (2000; see Figs. 3 and 4) indicates that much of what we are seeing is associated with regions of star formation. The same has been seen in other extragalactic star-forming regions by Alonso-Herrero et al. (2006). In general, these clumps as well as much of the emission outline the twin parallel lanes of emission seen as part of the large-scale warped disk in the lower resolution *Spitzer* mid-IR data (Quillen et al. 2006a, Fig. 1). At 8.8 μm and *N* band the Paα clumps C, D, E, F, and G seen by Schreier et al. (1998) are all detected along the direction of the top lane of emission seen by *Spitzer*. Along the bottom lane only the Paα clump K is detected. Several other mid-IR sources of emission associated with regions of Paα emission are also obvious in Figures 3 and 4. At 18.3 μm little evidence of this emission is seen. This is most likely for two reasons: (1) the lower sensitivity of the 18 μm (Qa) filter and (2) star formation regions typically having a PAH component at 8.6 and 11.3 μm that is readily detected in the 8.8 μm and *N*-band filters. However, at both 8.8 μm and *N* band some Paα clumps are devoid of mid-IR emission. Unfortunately this may be due to the limited chop throw ($15''$) of the data discussed above, which is certainly chopping onto other regions of low-level emission creating negative areas in the field of view. Thus, extensive analysis of theses star formation regions is not feasible at this time. However, there is an overall good correspondence between the Paα and mid-IR.

4.2.2. *Extended: Narrow-Line Region (NLR) Dust*

Although the nucleus can be heated entirely by the AGN it is unlikely that the bulk of the extended emission could be heated by the central engine. This low-level extended mid-IR emission, in some cases up to $10''$ (170 pc) away from the nucleus, would have to be extremely cool, on the order of $\sim$60 K assuming the same simple formula as in § 4.1.2. Assuming a normal blackbody SED of dust this cool, however, would cause significant emission (on the order of a few janskys) at longer wavelengths such as 18.3 μm, where no significant extended emission is seen on scales $>3''$. This provides further evidence that much of this mid-IR emission, especially that coincident with the Paα emission, is associated with local stellar activity.

The only significant 18.3 μm emission detected is a small clump of emission at a distance of $2.8''$ (48 pc) from the nucleus (P.A. $= 64^\circ$, measured north through east) approximately coincident with Paα clump A from Schreier et al. (1998; see Fig. 3). Krajnović et al. (2007) suggest this clump as well as clump B may be due to jet-induced star formation. Emission is detected in both clumps at 8.8 μm, while there is a $\sim 2\,\sigma$ detection of clump B at 18.3 μm. If this mid-IR emission is truly associated with shock-induced star formation regions, then we would expect heating of the surrounding dust to be local.

We measure the flux density in a $2''$ diameter area near clump A to be $\sim$4 mJy at 8.8 μm and $\sim$40 mJy at 18 μm; given the possibility of emission being chopped onto these, they can be considered rough estimates. Near clump B the mid-IR emission is similar to that of clump A, $\sim$4 mJy at 8.8 μm with very little emission ($\sim$17 mJy) at 18.3 μm. This results in an optically thin estimate of the temperature of 150–200 K near clump A and even warmer near clump B, which is farther away at $3.5''$ (60 pc). Given that we estimate that 14 pc is approximately the maximum distance that the AGN ($2.5 \times 10^9\ L_\odot$) can heat dust to 200 K this would rule out mid-IR emission near clump B as being centrally heated dust. Even for clump A at a temperature of 150 K only the smallest grains of graphite (0.003–0.005 μm) could be heated by the central engine. Although these are very simple estimates they do imply that local heating of dust due to shock-induced star formation associated with the radio ejecta is a possible explanation for mid-IR emission near clumps A and B. However, if there is an enhancement in luminosity in the direction of the NLR along the radio axis (northeast of the nucleus), as would be the case if the ionizing luminosity were anisotropic, then it may be possible to heat dust out to a radius consistent with clumps A and B. This could also explain the faint mid-IR extension seen on the opposite side (southwest of the nucleus) at 8.8 μm. This is thought to be the case in NGC 4151 (Radomski et al. 2003), where extended mid-IR emission on either side of the nucleus along the radio axis is thought to arise from a dusty NLR within the ionization cone heated by the central engine. In this case the NLR of NGC 4151 may see an ionizing luminosity a factor of $\sim$13 times greater than that seen from Earth (Penston et al. 1990). Anisotropies and beaming along the NLR have been predicted as strong as 200 times in some galaxies (Baldwin et al. 1987). In Cen A a beaming factor or underestimate of the true

luminosity of 10–20 times would be needed to be consistent with the central heating of clumps A and B within an ionization cone.

4.2.3. *Extended: Dusty Torus*

CO and H_2 measurements of Cen A show a nuclear ring of outer radius 80–140 pc, with an inner hole of diameter 40 pc enclosing a mass of $10^9\,L_\odot$ (Israel et al. 1990, 1991; Rydbeck et al. 1993; Marconi et al. 2001a). This ring is aligned perpendicular to the radio jet and has been speculated to be associated with the very outer parts of a torus. This would seem to contradict our earlier results which indicate a highly compact torus <3.5 pc. The difference, however, is entirely due to what is defined as the "torus" in AGNs. Shi et al. (2006) describes the "torus" as a multilayered system with an "inner" (<0.1 pc), "middle" (0.1–10 pc), and "outer" (10–300 pc) structure. In this scenario the compact tori seen in the mid-IR would typically correspond to the "middle" disk while the CO/H_2 is associated with the "outer" disk. Similar to Cen A, NGC 1068 also contains a compact mid-IR torus <15 pc (Mason et al. 2006) surrounded by a large 100 pc scale CO disk. Mid-IR polarization observations of NGC 1068 by Packham et al. (2007) provide continuity between these structures suggesting that the compact geometrically and optically thick torus is often surrounded by a larger and more diffuse structure associated with the dusty central regions of the host galaxy. Other dusty structures such as nuclear galactic bars may further merge into this scenario. Observations by Marconi et al. (2001b) even suggest that the H_2 structure shows kinematical evidence consistent with a galactic bar fueling the AGN, although they cannot entirely rule out a disk/torus structure.

Possible evidence for mid-IR emission associated with this "outer" torus/nuclear bar can be seen at both 8.8 μm and *N* band (Figs. 3 and 4). At both wavelengths there appears to be a ridge of emission extending up from the northwest of the nucleus toward Paα clump G. At 8.8 μm some mid-IR emission is also seen on the southeast side. In all cases this emission seems devoid of corresponding Paα emission associated with stellar activity as discussed earlier. Given that the data at 8.8 μm and *N* band are chopping on different areas of the galaxy (see § 2) it is unlikely that at least the northwest structure seen at both wavelengths is excessively distorted due to improper chop subtraction. This structure possibly indicates that the emission detected in CO/H_2 contains a dusty component. However, using simple calculations from § 4.1.2, even dust as small as 0.003 μm at this distance (5″–7″) would have to be on the order of 70–80 K to be heated by the central AGN. This is not reasonable as such cool dust should emit substantially more (on the order of a few janskys) at 18 μm where no significant emission is detected along this ridge. A more likely possibility is this emission is due to PAH emission as detected by *ISO* and *Spitzer* at least at 8.8 μm and possibility also at 11.3 μm in the *N* band.

NICMOS imaging by Schreier et al. (1998) shows a $1'' \times 2''$ (20 pc radius) emission line region interpreted as a gaseous disk also possibly associated with a multilayered torus which is nearly parallel to the radio jet and perpendicular to the CO disk. Schreier et al. (1998) hypothesized this peculiar angle may be caused by one of two scenarios: Either it had formed recently enough (possibly associated with a merger or infall event) such that it had not time to become aligned with the black hole spin axis, or because it was along the major axis of the bulge it was dominated by the galaxy gravitational potential rather than that of the black hole. In either case these observations indicate that there may be an outer gaseous ring of material that is highly warped with respect to the inner compact mid-IR torus. Although we do generally detect low-level mid-IR emission along this direction we detect no extension associated with this structure at the level of the FWHM.

4.2.4. *Extended: Synchrotron Emission*

As discussed earlier, in both epoch A and B data extended mid-IR emission is detected approximately coincident with Paα clumps A and B from Schreier et al. (1998). This emission also falls very near the axis of the powerful radio jet in Cen A. At *N* band especially (Fig. 4) emission is seen along the inner part of the radio jet extending out past the Paα clumps A and B. As discussed above it is difficult to rule out shock-induced star formation and/or dusty NLR emission. Furthermore, due to the possibility of inadequate chop-subtraction, attempting to fit a synchrotron model to evaluate its contribution, if any, is difficult. Thus, we cannot confirm nor rule out some contribution from synchrotron radiation emanating from the jet near the nucleus. Farther out along the jet axis in the northeast direction negative emission from improper chop subtraction becomes more apparent in both epoch A and B data and some faint mid-IR emission associated with the jet is most likely lost. However, in epoch B at *N* band there is clear evidence of mid-IR emission located farther out and coincident with the radio axis. This new source is denoted as RPL 1 (Fig. 4).

RPL 1 is located in a very bright area of the radio jet at a distance of 18.4″ (P.A. $= 53^\circ$, measured north to east). It is outside the field of view of the epoch A data and thus cannot be characterized at 8.8 and 18.3 μm. Given the distance as projected on the sky, $18.4'' \geq 300$ pc. This rules out dust heated by the central source, as it would take a beaming factor of >500 to heat even the smallest dust grains to a temperature of 200 K. If no beaming is assumed the maximum temperature that a blackbody heated by the central AGN could obtain at that distance is 42 K, which given an approximate flux density of 2 mJy at *N* band would require a 25 μm flux several hundred thousand times what is measured by *IRAS*. Confidence in the detection of this source is strong as it is seen on all three nights observed at *N* band and after a 20 pixel (1.78″) offset/dither between nights. Stacking all three nights of data results in a 3–4 σ detection (Fig. 4). Mid-IR emission from a synchrotron jet has been seen in M87 (Perlman et al. 2001) and at larger radii from Cen A by *Spitzer* (HKW06), but in these cases the mid-IR morphology and position showed a strong spatial and morphological correspondence to that of the radio emission from the jet. This does not seem to be the case in RPL 1, which is located offset $\sim 2''$ from a bright radio knot and has a much less elongated shape. Another possible explanation is a dusty clump heated by the impact or shock of the outflow impinging on surrounding material associated with jet-induced star formation. However, it is possible that the morphology of this weak source is affected by improper chop subtraction of the crowded mid-IR emission in Cen A, and thus it requires further investigation.

5. CONCLUSIONS

We detect a bright unresolved mid-IR nucleus surrounded by low-level emission in the central region of Centaurus A. We find the bright central nucleus of Cen A to be unresolved in the mid-IR at the level of the FWHM. Using multiple PSF measurements and their variation, we place an upper limit on the size of the mid-IR nucleus of Cen A of 3.2 pc (0.19″) at 8.8 μm and 3.5 pc (0.21″) at 18.3 μm. This is consistent with our models, which predict the mid-IR emission from a torus in Cen A to be unresolved

with a size of 0.05″ or less. The primary source of the nuclear mid-IR emission is likely to be associated with this dusty torus and NLR emission with minimal contributions from starburst and synchrotron emission.

Extended mid-IR emission in Cen A is generally coincident with Paα regions most likely due to stellar activity. A ridge of mid-IR emission perpendicular to the radio axis and devoid of much Paα emission may be associated with a CO and H_2 outer ring/bar. Emission associated with Paα clumps A and B from Schreier et al. (1998) could be due to shock heating or possibly centrally heated dust in a NLR if anisotropic beaming of radiation along the radio axis is taken into account. A new mid-IR source, RPL 1, is detected along the radio axis at a distance of 18.4″ (P.A. = 53°) and is possibly due to shock heating of material impacted by the jet or synchrotron emission. Overall the mid-IR emission in the nuclear region is shown to be very complex and in need of further study.

J. T. R., J. M. D., and R. M. acknowledge the support of the NSF. This work is based on observations obtained at the Gemini Observatory, which is operated by the Association of Universities for Research in Astronomy, Inc., under a cooperative agreement with the NSF on behalf of the Gemini partnership: the National Science Foundation (United States), the Particle Physics and Astronomy Research Council (United Kingdom), the National Research Council (Canada), CONICYT (Chile), the Australian Research Council (Australia), CNPq (Brazil), and CONICET (Argentina). We also thank Matthew Sirocky for his assistance with the torus simulations, and N. A. L. acknowledges support from NSF award AST 02-37291. J. T. R. would also like to acknowledge Craig Markwardt for his very useful IDL routines which were used to fit Moffat profiles and Alessandro Marconi for trying to find his original Paα images. C. P. would like to acknowledge NSF grant 0206617. All authors would also like to thank the referee for the helpful comments that improved this paper.

REFERENCES

Abraham, Z., Kaufmann, P., & Botti, L. C. L. 1982, AJ, 87, 532
Alexander, D. M., Efstathiou, A., Hough, J. H., Aitken, D. K., Lutz, D., Roche, P. F., & Sturm, E. 1999, MNRAS, 310, 78
Alonso-Herrero, A., Colina, L., Packham, C., Díaz-Santos, T., Rieke, G. H., Radomski, J. T., & Telesco, C. M. 2006, ApJ, 652, L83
Antonucci, R. 1993, ARA&A, 31, 473
Baldwin, J. A., Wilson, A. S., & Whittle, M. 1987, ApJ, 319, 84
Beall, J. H., et al. 1978, ApJ, 219, 836
Becklin, E. E., Frogel, J. A., Kleinmann, D. E., Neugebauer, G., Ney, E. P., & Strecker, D. W. 1971, ApJ, 170, L15
Capetti, A., et al. 2000, ApJ, 544, 269
Chiaberge, M., Capetti, A., & Celotti, A. 1999, A&A, 349, 77
———. 2001, MNRAS, 324, L33
Clarke, D. A., Burns, J. O., & Norman, M. L. 1992, ApJ, 395, 444
Draine, B. T., & Lee, H. M. 1984, ApJ, 285, 89
Evans, A. S., et al. 2003, AJ, 125, 2341
Grasdalen, G. L., & Joyce, R. R. 1976, ApJ, 208, 317
Groves, B., Dopita, M., & Sutherland, R. 2006, A&A, 458, 405
Häring-Neumayer, N., Cappellari, M., Rix, H.-W., Hartung, M., Prieto, M. A., Meisenheimer, K., & Lenzen, R. 2006, ApJ, 643, 226
Hardcastle, M. J., Kraft, R. P., & Worrall, D. M. 2006, MNRAS, 368, L15 (HKW06)
Hardcastle, M. J., Worrall, D. M., Kraft, R. P., Forman, W. R., Jones, C., & Murray, S. S. 2003, ApJ, 593, 169
Israel, F. P. 1998, A&A Rev., 8, 237
Israel, F. P., van Dishoeck, E. F., Baas, F., de Graauw, T., & Phillips, T. G. 1991, A&A, 245, L13
Israel, F. P., van Dishoeck, E. F., Baas, F., Koornneef, J., Black, J. H., & de Graauw, T. 1990, A&A, 227, 342
Karovska, M., et al. 2003, ApJ, 598, L91 (K03)
Kleinmann, D. E., & Wright, E. L. 1974, ApJ, 191, L19
Krabbe, A., Böker, T., & Maiolino, R. 2001, ApJ, 557, 626
Krajnović, D., Sharp, R., & Thatte, N. 2007, MNRAS, 374, 385
Krolik, J. H., & Begelman, M. C. 1988, ApJ, 329, 702
Laor, A., & Draine, B. T. 1993, ApJ, 402, 441
Lepine, J. R. D., Braz, M. A., & Epchtein, N. 1984, A&A, 131, 72
Marconi, A., Capetti, A., Axon, D., Koekemoer, A., Macchetto, D., & Schreier, E. 2001a, Mem. Soc. Astron. Italiana, 72, 47
———. 2001b, ApJ, 549, 915
Marconi, A., Pastorini, G., Pacini, F., Axon, D. J., Capetti, A., Macchetto, D., Koekemoer, A. M., & Schreier, E. J. 2006, A&A, 448, 921
Marconi, A., Schreier, E. J., Koekemoer, A., Capetti, A., Axon, D., Macchetto, D., & Caon, N. 2000, ApJ, 528, 276
Mason, R. E., Geballe, T. R., Packham, C., Levenson, N. A., Elitzur, M., Fisher, R. S., & Perlman, E. 2006, ApJ, 640, 612
Mason, R. E., Levenson, N. A., Packham, C., Elitzur, M., Radomski, J., Petric, A. O., & Wright, G. S. 2007, ApJ, 659, 241
Meisenheimer, K., et al. 2007, A&A, 471, 453
Meurer, G. R., Heckman, T. M., Lehnert, M. D., Leitherer, C., & Lowenthal, J. 1997, AJ, 114, 54
Mirabel, I. F., et al. 1999, A&A, 341, 667
Moffat, A. F. J. 1969, A&A, 3, 455
Nenkova, M., Ivezić, Ž., & Elitzur, M. 2002, ApJ, 570, L9
Packham, C., Hough, J. H., Young, S., Chrysostomou, A., Bailey, J. A., Axon, D. J., & Ward, M. J. 1996, MNRAS, 278, 406
Packham, C., Radomski, J. T., Roche, P. F., Aitken, D. K., Perlman, E., Alonso-Herrero, A., Colina, L., & Telesco, C. M. 2005, ApJ, 618, L17
Packham, C., et al. 2007, ApJ, 661, L29
Penston, M. V., et al. 1990, A&A, 236, 53
Perlman, E. S., Sparks, W. B., Radomski, J., Packham, C., Fisher, R. S., Piña, R., & Biretta, J. A. 2001, ApJ, 561, L51
Quillen, A. C., Bland-Hawthorn, J., Brookes, M. H., Werner, M. W., Smith, J. D., Stern, D., Keene, J., & Lawrence, C. R. 2006a, ApJ, 641, L29
Quillen, A. C., Brookes, M. H., Keene, J., Stern, D., Lawrence, C. R., & Werner, M. W. 2006b, ApJ, 645, 1092
Quillen, A. C., Graham, J. R., & Frogel, J. A. 1993, ApJ, 412, 550
Radomski, J. T. 2003, Ph.D. thesis, Univ. Florida
Radomski, J. T., Piña, R. K., Packham, C., Telesco, C. M., De Buizer, J. M., Fisher, R. S., & Robinson, A. 2003, ApJ, 587, 117
Radomski, J. T., Piña, R. K., Packham, C., Telesco, C. M., & Tadhunter, C. N. 2002, ApJ, 566, 675
Rydbeck, G., Wiklind, T., Cameron, M., Wild, W., Eckart, A., Genzel, R., & Rothermel, H. 1993, A&A, 270, L13
Sako, S., et al. 2003, PASP, 115, 1407
Schreier, E. J., et al. 1998, ApJ, 499, L143
Sellgren, K., Werner, M. W., & Dinerstein, H. L. 1983, ApJ, 271, L13
Shi, Y., et al. 2006, ApJ, 653, 127
Siebenmorgen, R., Krügel, E., & Spoon, H. W. W. 2004, A&A, 414, 123
Silge, J. D., Gebhardt, K., Bergmann, M., & Richstone, D. 2005, AJ, 130, 406
Soifer, B. T., et al. 2000, AJ, 119, 509
———. 2001, AJ, 122, 1213
Soifer, B. T., Bock, J. J., Marsh, K., Neugebauer, G., Matthews, K., Egami, E., & Armus, L. 2003, AJ, 126, 143
Telesco, C. M. 1978, ApJ, 226, L125
Telesco, C. M., Pina, R. K., Hanna, K. T., Julian, J. A., Hon, D. B., & Kisko, T. M. 1998, Proc. SPIE, 3354, 534
Urry, C. M., & Padovani, P. 1995, PASP, 107, 803
Weedman, D. W., et al. 2005, ApJ, 633, 706
Weingartner, J. C., & Draine, B. T. 2001, ApJ, 548, 296
Whysong, D., & Antonucci, R. 2004, ApJ, 602, 116